JOURNAL OF AGRICULTURAL AND FOOD CHEMISTRY

J. Agric. Food Chem. **2006,** *54,* 597−606 **597**

The Maize Primary Cell Wall Microfibril: A New Model Derived from Direct Visualization

SHI-YOU DING* AND MICHAEL E. HIMMEL

National Bioenergy Center, National Renewable Energy Laboratory, 1617 Cole Boulevard, Golden, Colorado 80401

Understanding the molecular architecture of the plant cell wall is critical to reducing the biomass recalcitrance problem, which currently impedes economic bioconversion processing. The parenchyma cell walls from field senesced, maize stem pith have been directly visualized without extraction processes using high-resolution atomic force microscopy (AFM). By imaging the cell wall inner surfaces from different cells and different faces of the same cell, we were able to map the native primary cell wall ultrastructures. Depending on the thickness of non-cellulosic deposition, the parallel-microfibrils appear in various morphologies ranging from clearly defined to completely embedded in the wall matrixes forming cell wall lamella. Macrofibrils were found to exist only on the uppermost layer of the native primary cell wall and appeared to be bundles of elementary fibrils. This novel observation led us to a new hypothesis for the cell wall fibrillar network and biosynthesis processes. Put concisely, a number of elementary fibrils are synthesized at one locus, that of the cellulose synthase complex (CelS), and coalesce into much larger macrofibrils. These macrofibrils eventually split at the ends to form parallel microfibrils with deposition of other cell wall components (i.e. hemicelluloses, pectin, etc.) also evident. On the basis of these AFM surface measurements and current supportive evidence from cell wall biophysics, biosynthesis, and genomics, we propose a new molecular model consisting of a 36-glucan-chain elementary fibril, in which the 36-glucan chains form both crystalline and subcrystalline structures. We also propose a modified model of CelS based on recently reported experimental evidence from plant cell wall biosynthesis.

KEYWORDS: Microfibril; elementary fibril; maize, cellulose; plant cell wall; atomic force microscopy

INTRODUCTION

To enable a new biorefinery industry, we must overcome the natural recalcitrance of lignocellulosic biomass to deconstruction. Deeper understanding of these mechanisms will permit improvements in the process of converting biomass (plant cell walls) to fermentable sugars and eventually bioethanol. Maize was chosen for this study because of the significant potential this crop represents for near term biomass conversion processes and its suitability as an ultrastructural model for other potential monocotyledon crop plants. For example, current annual production of corn stover in the U.S. is about 250M tons/year, from which about 75M tons/year can be collected and made available for ethanol production (about 4 to 6B gallons/year) (*1*).

Plant cell walls are complex and dynamic structures mostly composed of cross-linked polysaccharide networks, glycosylated proteins, and lignin. The molecular architecture and biosynthesis of higher-plant cell walls remains one of the greatest challenges in plant science today. Most plant cell wall models now view these structures as a type of polymer liquid crystal (PLC) where cellulose fibril networks are embedded in non-cellulosic polysaccharide matrixes (hemicelluloses and pectin), composed with lignin, and structural proteins (*2*−*4*). Among these cell wall components, cellulose is considered to be the only crystalline mesogen in the plant cell wall PLC system (*5*). Cellulose is the dominant polysaccharide in plant cell walls and often touted as "the most abundant biopolymer on earth". Most experimental evidence reported today suggests that cellulose in higher plants is synthesized on the cell membrane of growing plant cells from hexagonal arrays of cellulose synthase complexes (CelS), known as rosettes (*6*). The CelS complex synthesizes a basic cellulose unit, known as the elementary fibril, which contains 36 β-D-glucan chains, and may eventually be coated with non-cellulosic polysaccharides to form the cell wall microfibril (*7*). These microfibrils are then cross-linked by hemicelluloses/pectin matrixes during cell growing (*2*, *3*). Considerable progress has been made recently in the discovery of genes related to cellulose biosynthesis. In particular, the expression patterns and transcriptional profiles of these genes have been analyzed in mutants of *Arabidopsis thaliana* and a few other monocots and some dicots. This work has provided new insights into the function and biosynthesis of plant cell walls, reviewed by Doblin and co-workers (2002) (*8*). However, detailed definitive evidence

* To whom correspondence should be addressed. Telephone: 303-384-7758. Fax: 303-384-7752. E-mail: shi_you_ding@nrel.gov.

10.1021/jf051851z CCC: $33.50
Published on Web 01/17/2006

is not yet available from biophysics for many aspects of microfibril biosynthesis in plant cell walls (*4*). In this report, we focus on one of these fundamental problems: the molecular structure of the microfibril and its biosynthesis. We evaluate recent experimental studies of the plant cell wall and combine this understanding with our own high-resolution direct imaging techniques. We also review current knowledge gaps and propose a modified model of microfibril molecular structure and its biosynthesis.

The plant cell wall microfibril is commonly measured by conventional transmission electron microscopy (TEM). The sizes of the microfibrils from different plant tissue and species are estimated to be from 2 to 10 nm in diameter (*9*−*11*). This apparent variation may come not only from the diversity of plant species and cell types, but also from the limitations of the TEM technique. For example, different sample preparation methods could also generate different apparent diameters of the microfibrils because of simple aggregation (*12*). Also, it may be essentially impossible to completely remove the non-cellulose polysaccharides that are closely associated with the crystalline cellulose. For example, alkaline treatment conditions known to solubilize hemicellulose could also cause fiber aggregation (*13*) or convert native cellulose I to cellulose II (*14*). Indeed, during sample preparation processes used for conventional TEM, most of the hemicelluloses in the microfibril are extracted. Still, this "treated microfibril" has often been considered equivalent to the actual elementary fibril, and this may be erroneous.

From TEM measurements, the cross section of the treated microfibril has been reported to be essentially rectangular, with dimensions of 2×3 nm^2 (*10*). Actually, the cross section of the native *Valonia* cellulose crystal appears to be hexagonal under high-resolution scanning TEM (*15*) (Ding et al., unpublished data). Therefore, the dimensions of the cellulose crystal measured by TEM could also be different when the crystal stands on different edges. The size of the small cellulose crystallite estimated from TEM is consistent with that measured by other methods, including ^{13}C solid-state NMR (*11*, *16*), X-ray diffraction, small angle neutron scattering (SANS) (*17*), and FTIR spectroscopy (*18*). Furthermore, cellulose content is thought to vary between the primary wall and the secondary wall; however, the size of the cellulose crystallite of each microfibril appears to be constant across many cell wall sources. Biophysical studies have also confirmed that the microfibril contains both crystalline and paracrystalline regions (*19*). Both NMR and FTIR spectroscopy have suggested that plant cell wall crystalline cellulose contains regions exhibiting highly disordered (subcrystalline) structures (*16*). It is clear that the crystal structure of cellulose in microfibrils and the interaction between cellulose and non-cellulosic polysaccharides in cell walls are not well understood.

Recently, the crystal structures of native cellulose (cellulose I) were determined from the algae *Glaucocystis* (Iα, triclinic) (*20*) and the tunicate *Halocynthia roretzi* (Iβ, monoclinic) (*21*). These two crystal allomorphs naturally coexist in various proportions in different organisms. Traditionally, higher-plant cell wall cellulose was believed to consist primarily of a Iβ-like form of cellulose and a small proportion of Iα-like cellulose (*22*, *23*). However, solid-state ^{13}C NMR spectroscopy has suggested that in higher plants there is only the Iβ crystalline allomorph with disordered chains immediately associated with its crystallite surface (*24*).

AFM has been used increasingly to characterize biological samples because of several obvious advantages. First, measurements can be made in nearly an *in vivo* physiological environment (in air or under fluid), which is essential to eliminate structural modifications generated during sample preparation. Second, high-resolution, i.e., atomic resolution, is possible. AFM imaging is thus compatible with the resolution of the TEM. Third, it is possible to obtain sample topography (height image) and elasticity (phase image) data simultaneously. Most uncertainty for AFM measurements stems from scanning artifacts that cause apparent image broadening. These artifacts however, have recently been significantly minimized with better probe control, more accurate calibration, and new probes with reproducibly sharper tips (as small as 1 nm). Direct visualization of the cellulose crystal (*25*, *26*) and plant cell wall surface using AFM has revealed higher resolution and more accurate measurement of microfibrils (*27*−*29*). In this study, we chose the parenchyma cells from field senesced, maize (*Zea mays L.*) stem pith as a representative cell type for AFM analysis at the molecular and submolecular level. The goal of this research was to directly characterize and visualize the primary cell wall with few or no preparation steps.

To simplify the discussion in this report, "cellulose" refers only to the β-(1,4)-D-glucans. In biology, the term for cellulose usually refers to a heterogeneous mixture of biopolymers that include crystalline cellulose, noncrystalline β-D-glucans, and various amounts of hemicelluloses. We use the term "elementary fibril" to describe the original strand synthesized by the cellulose synthase complex. "Microfibril" refers to a microscopic feature, which is a morphological unit containing one elementary fiber and probably immediately associated non-cellulosic polymers. We propose that the bundle of elementary fibrils, which can be visualized using scanning EM at low resolution, actually describes a structure we call the "macrofibril."

MATERIALS AND METHODS

Sample Preparation. Field-dried Mo17 maize (corn stover) was harvested from Madison, WI, in the late fall of 2003. Using a binocular stereomicroscope, parenchyma cells were separated using a single blade razor from the pith of internode sections taken from the upper one-third of the stem. Single cells were collected and suspended in water, wetted small pieces of cell wall were then applied to a glass cover slide, extra water was removed using a piece of filter paper, and the sample was air-dried. The sample was first imaged with an inverted microscope with a high-resolution digital camera (Olympus IX71 with DP70 digital camera, Melville, NY) to ensure that a single layer of the cell wall was perfectly fixed.

AFM Measurement. A Multi-Mode scanning probe microscope (SPM) with a NanoScope IV controller (Veeco, Santa Barbara, CA) was utilized for all AFM measurements. To ensure absolute stability, the AFM was located in a specially designed laboratory with acoustic and vibration isolation. A customized Nikon optical microscope with deep focus (maximum 800× magnification) was used to aid the positioning of the AFM tip to the desired face and location on the cell wall. For most experiments, the standard 15-μm scanner was used with the TappingMode etched silicon probes (TESP, Veeco NanoProbe) or the aluminum-coated probes (HI'RES, MikroMasch, Portland, Oregon). We used an autotuning resonance frequency range of 250−300 kHz and a scan rate of 0.5−3 Hz. The drive amplitude and set point were adjusted during measuring to minimize tip artifacts. Colloid gold particles (5, 10, 15, 20, and 30 nm diameter) were used to calibrate the AFM (Gold Calibration Kit, Ted Pella, Inc., Redding, CA). The software Nanoscope 6.12r1 was used for AFM operation and later imaging processing.

RESULTS

AFM measures attractive and repulsive forces between the scanning probe tip and the sample surface to generate a 3-D map or replica of the surface. AFM can thus provide images of

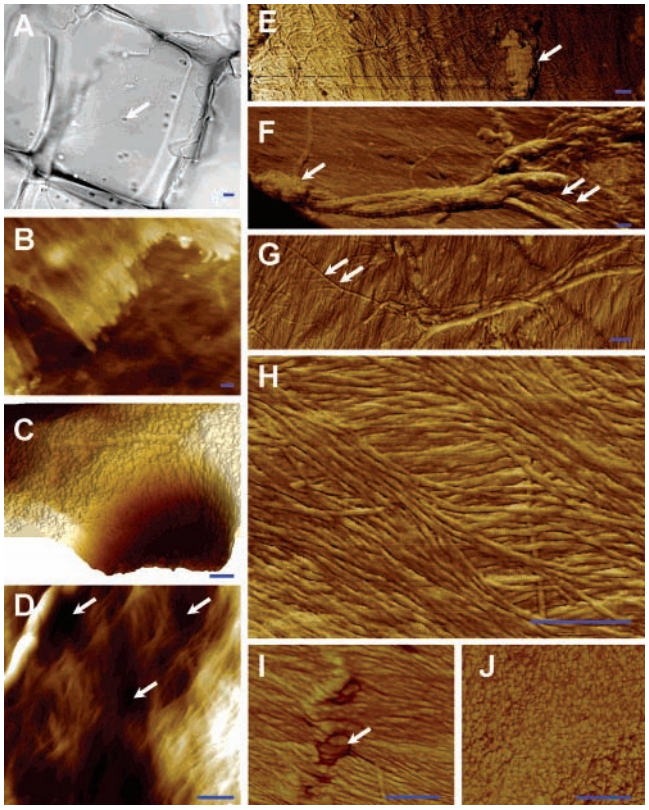

Figure 1. Primary cell walls from maize parenchyma. **(A)** A light microscopy image shows a fairly transparent primary wall with primary pits (white arrow), bar = 10 μm. **(B–J)** AFM mapping of wall surfaces, bar = 200 nm: wall lamellae (**B**, height image); primary pit (**C**, 3-D image); pit-field (**D**, height image); dried cytoplasm remnants or membrane debris (**E**, phase image); a process of synthesis of elementary fibrils–macrofibrils–micrifibrils [the elementary fibrils are synthesized from one point (white arrow)] (**F**, phase image); a number of elementary fibrils coalesce into a macrofibril, which splits/branches into microfibrils (double white arrow) (**G**, phase image); newer synthesized sheets of parallel-oriented microfibrils (**H**, phase image); microfibrils coated with more non-cellulosic polymers, and particles (structural protein?) embedded in the matrixes (**I**, phase image); and more cell wall components deposited in the wall matrixes (microfibrils are hardly visible) (**J,** phase image).

the topology and elasticity of a complex sample surface at high resolution. AFM accuracy always depends on the performance of the tip used during the measurement. Tip size, shape, and irregularities can generate artifacts, especially when imaging complex "three-dimensional" samples such as plant cell walls (*27*). We employed several techniques to minimize this problem. First, we calibrated each new tip using different sizes of gold particles. Second, we used a light microscope with a high-resolution digital camera attached to the AFM to reproducibly locate the tip and sample. Third, we used new (and different) tips to measure the same surface areas. Fourth, we used a constant-scan-size strategy to ensure reproducibility. For example, we started scanning with the higher resolution scan (200 $\times$ 200 nm^2) and systematically rescanned with larger scan dimensions (1 $\times$ 1 μm^2, 2 $\times$ 2 μm^2, 5 $\times$ 5 μm^2, 10 $\times$ 10 μm^2, 15 $\times$ 15 μm^2), using the same relative scan rate and monitoring the roughness of the different scanning dimensions. We also rotated the scan direction by 45° and 90° while keeping all other settings the same (repeating the scan at least twice).

The parenchyma cell from maize stem pith has a typically polyhedral-shaped wall and is 150−200 μm in diameter. In light microscopy (**Figure 1A**), the thin nonlignified cell walls shown are relatively transparent and feature primary pits. Using the AFM measurement as described above, we were able to image different areas on one face, as well as different faces of a single cell. More than fifty parenchyma cell walls were imaged. For a given piece of cell wall, using the "autoscan" function of Nanoscope IV, the maximum amount of pictures was taken to cover the entire surface. **Figure 1** shows representative pictures of the parenchyma cell wall surface chosen from over 500 AFM images taking from different cell walls. In most cases, the primary walls appear rather "clean" with sheets of fibers apparent (**Figure 1B and H**). What appears to be dried cytoplasm remnants or membrane debris or both can be detected in large scanning areas. These structures are normally hundreds of nanometers in size (**Figure 1E**). We also observed occasional cell wall depressions (**Figure 1C**) and rugae, which form the general cell wall landscape. The rugae are about 2−3 μm long, 100 nm high, and 100 nm wide. Insertion of particle-like materials between the lamellae could also cause this ridge effect (**Figure 1I**). We noted two different types of cell wall depressions: primary pits (**Figure 1C**) and primary pit-fields (primordial pits, **Figure 1D**) appear on different cell walls. The "well-shaped" primary pit is approximately 2 μm wide and 150−200 nm deep. **Figure 1C** shows a 3-D image of one primary pit rendered from an AFM height image. The pit-field is a community of small wall depressions (plasmodesma) readily apparent (**Figure 1D**).

Parenchyma is usually composed of living cells displaying primary walls. Thin wall layers of secondary deposition are commonly observed during cell growth. **Figure 1B** shows wall lamellae at the broken edge. The thickness of each lamella is approximately 10 nm, measured from the AFM height image. There also appears to be only one microfibril sheet in each lamella (**Figure 1H**). These microfibrils are arranged in parallel sheets and rotated approximately 50° with respect to each other. The surface roughness appears different at the nanometer level on different cell wall faces. By imaging different wall faces, the microfibrils range in appearance from clearly defined (**Figure 1H**) to fully embedded in the cell wall matrixes (**Figure 1I and J**). We also found that, on a given cell wall face, the microfibrils appear uniform and parallel. The length of each microfibril was usually tens of micrometers, which corresponds to the full face of the cell wall. The surfaces of these microfibrils were rather smooth with no detectable periodicity along the long axis. As measured from our AFM images from different walls, the dimensions of the cross sections of the microfibrils may vary in walls from cell to cell. In the case of clearly defined microfibrils, the cross section of the microfibrils was found to be 3 $\times$ 5 nm (**Figure 1H**). In other cases, microfibrils appeared to be heavily coated (**Figure 1I**), even to the point of becoming invisible (**Figure 1J**). In addition, numerous particles (20−50 nm in diameter) embedded between the microfibril layers can be observed in **Figure 1I**. These particles could be cell wall proteins.

An interesting observation from this study is the macrofibrils, which appear to be bundles of smaller fibers. These structures seem to exist only on the uppermost surface of some parenchyma cell walls (**Figure 1F and G**) and are not found in the cell walls where the microfibrils appear to be heavily coated with what we presume are hemicelluloses/pectin matrixes (**Figure 1I and J**). Unlike the parallel microfibrils, the macrofibrils appear to orient randomly on the cell wall surface (**Figure 2**). The size of the macrofibril varies from 50 to 250 nm in diameter (**Figure 1F and G**, **Figure 2**). **Figure 1F** shows a large macrofibril starting from one locus where an unidentifi-

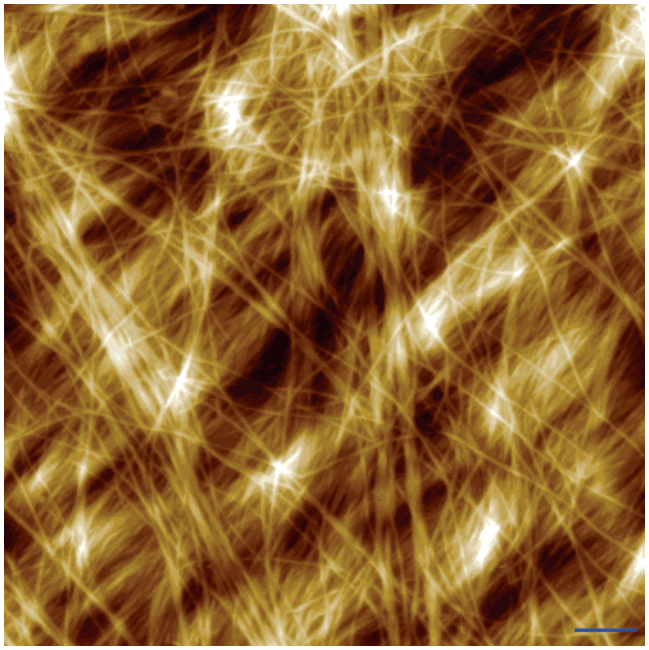

Figure 2. High-resolution AFM height image showing a typical primary cell wall surface structure. Microfibrils are parallel-arranged, and the macrofibrils scatter only on the wall surface. Bar = 200 nm.

able, featureless structure is also detected. Could those be cellulose synthase complexes? In this image, the macrofibril appears to "split" or untangle at the right end to form a set of smaller parallel fibers, which we assume are microfibrils (**Figure 1G and H**). The morphology of fibers in the macrofibril appears to be faceted, which differs from that of the microfibril (**Figure 1F**). **Figure 1G** specifically shows that the macrofibril branches at the end.

DISCUSSION

Direct imaging using AFM offers a powerful tool to visualize the native cell wall surface at the molecular level, which provides new insights into understanding of plant cell wall structure and its biosynthesis. Parenchyma cells are believed to be primarily living cells that have dynamic walls during cell elongation. By analyzing cell wall morphology of different parenchyma cells, we were able to visualize the cell walls in different growing stages. As the cells expand, more cell wall components are deposited on the inner faces in a directional way. From correlations of our current AFM data with recently published discoveries in plant cell wall biosynthesis and biophysics, we have attempted to close some knowledge gaps about plant cell wall ultrastructure.

Cellulose Synthases—Clues from the Transcriptome. Most recent achievements in plant cell wall biosynthesis research resulted from the analysis of *Arabidopsis thaliana* cell wall phenotype mutants and genome sequence data (*4*,*8*). Most researchers agree that cellulose is synthesized in the plasma membrane, whereas hemicelluloses are assembled and secreted from the Golgi vesicles (*30*). More than 1000 genes have been putatively identified to be involved in plant cell wall biosynthesis (*4*). A few of these genes are believed to encode the cellulose synthases (CesA) that polymerize β-1,4-D-glucan. Genes encoding these CesA proteins were previously classified as family-2 processive glycosyltransferases (http://afmb.cnrs-mrs.fr/~cazy/CAZY/index.html). Signature features of the CesA proteins include *N*-terminal zinc finger domains, eight trans-membrane helix domains, and a conserved DDDQXXRW motif that may be responsible for the binding of the substrate uridine diphosphoglucose (UDP-GLC). A number of CesA genes have also been identified from other higher plant species using bioinformatics methods (http://cellwall.stanford.edu). Recent studies of the expression profiles of CesA genes have revealed cell-type specificity with differentially regulated expression patterns (*8*,*31*−*34*), which implies that different CesA proteins may play distinct roles in the cellulose biosynthesis. The relative abundance of mRNA transcripts of eight CesA proteins from barley has been analyzed using the quantitative polymerase chain reaction (Q-PCR) approach, which recognizes two groups of CesA genes as coordinately transcribed. The group I genes, including *HvCesA1*, *-2*, and *-6*, were expressed in most test tissues (leaf, root, floral, grain, coleoptile, and stem). The group II genes, including *HvCesA4*, *-7*, *-8*, were expressed only in maturing tissues (root, stem), so they are possibly involved in secondary wall synthesis. Interestingly, in most tested samples, the expression level of each CesA gene was different. The ratio of normalized expression levels of the three primary cell wall CesA genes was approximately *HvCesA6/HvCesA2/HvCesA1* = 1:2:3 (*31*). Similar coordinate transcriptional patterns could be predicted in other plant species; for example, the phylogenetic analysis of CesA genes from *A. thaliana* and *Hordeum vulgare* (barley), *HvCesA6*, *HvCesA2*, and *HvCesA1* group with *AtCesA1*, *AtCesA6*, and *AtCesA3*, respectively (*31*, *32*). Indeed, preliminary expression analysis shows that three CesA genes (*AtCesA1*, *AtCesA6*, and *AtCesA3*) are coexpressed in the same cell with primary cell walls, and the other three CesA genes are specifically coexpressed in xylem cells when secondary wall deposition starts. Furthermore, the transcript levels of these three primary wall genes (*AtCesA1*, *-6*, and *-3*) differ within the same cell (*34*). Arioli et al. (*35*) found that *AtCesA1* is expressed in most cell types and that the *rsw1* (*AtCesA1*) mutation significantly reduces both the cellulose content in cell walls and accumulation of noncrystalline β-(1,4)-D-glucan.

In summary, from these studies of the expression profiles of CesA genes and *A. thaliana* mutant analysis, at least three CesA proteins are required in primary cell wall synthesis. An additional group of CesA proteins is specifically expressed in secondary cell walls. Each CesA gene plays a different role, and at least one CesA gene, for example, *AtCesA1* in *A. thaliana*, may be critical for the synthesis of crystalline cellulose.

Rosette Assembly—Biochemical Clues. The cellulose synthase complex (CelS), known as rosettes in higher plants, was first observed using electron microscopy and the freeze−fracture sample preparation technique. Rosettes appear in hexagonal geometry with a honeycomb pattern arrayed in the plasma membrane (*36*, *37*). Rosettes are believed to be responsible for the synthesis of elementary fibrils in most current plant cell wall biosynthesis models (*7*). More recently, mutant analyses (reviewed by Doblin et al.) (*8*) and immunolabeling (*38*) have confirmed that the rosettes are composed of cellulose synthase (CesA) proteins and that at least three types of CesA isoforms (α1, α2, and β) are required for the spontaneous assembly of single rosettes. Examples include *AtCesA1*, *-6*, and *-3* from the primary cell wall of *A. thaliana* (*39*); *HvCesA6*, *HvCesA*2, and *HvCesA1* from barley (*31*); and *OsCesA4*, *-7*, and *-9* from rice (*33*). The next question is; how many CesA proteins are assembled into single rosettes? Having multiple CesA proteins coexpressed in the same cell does not necessarily mean that they are all assembled into the same rosettes (*40*). A model of rosettes has been proposed by Scheible and co-workers (*41*) and modified by Doblin and co-workers (*8*), in which the three types of CesAs (α1, α2, and β) are assembled hexagonally. In

this model, there are three types of positions available in each rosette corresponding to one α1, two α2, and three β isoforms, respectively. Among those three positions, the α1 is unique and may be responsible for the crystalline cellulose synthesis. A putative α1-type CesA must be (1) critical in wall synthesis, (2) expressed in all cell types, and (3) expressed at a relatively lower level (only one molecule is needed in a rosette subunit) than the α2 and β CesAs. For example, *AtCesA1* in *A. thaliana* and *HvCesA6* in barley could encode the α1-type of CesA protein (see discussion above). It is difficult to predict which CesA proteins fit into the α2 and β positions. In Scheible and Doblin's model, the β isoform could form α2−β−α2 or α1−β−α2 interactions, which may indicate that more than one CesA protein could potentially share the α2 or β position. The transcriptional analysis of CesA genes from barley seemed to support this prospective. Burton and co-workers (*31*) have showed that there are at least four CesA genes expressed in all tested tissues and that three additional specific CesA genes are expressed in secondary wall deposition. Each position (i.e. α1, α2, and β) in different rosettes may have different CesA proteins, or different CesA proteins may fit in the same type of position in one rosette. For example, there are three β positions in one subunit and 18 positions in one rosette (the β position might be occupied by different CesA enzymes).

In the Scheible and Doblin model, at least three types of protein−protein interaction are proposed: α2−β and α1−β to form each subunit, and α2−α2 between subunits to form rosettes. However, the rosettes are arrayed in the plasma membrane in a honeycomb pattern so another α1−α1 interaction would be predicted to be necessary to facilitate interaction among rosettes. To simplify this, we proposed a new modified model shown in **Figure 3**. In our model, each subunit in the previous model was rotated by 180° to create a β−β interaction; therefore, only three types of interaction are needed for the spontaneous assembly of rosettes in the plasma membrane: β−β, α1−β, and α2−β. The β−β interaction facilitates the assembly of six subunits into rosettes (**Figure 3B**), as well as the array of rosettes in the plasma membrane (**Figure 3C**). The six subunits of rosettes are identical, and each rosette is composed of one molecule of α1, two molecules of α2, and three molecules of β (**Figure 1A**). We believe our simplified rosette model seems probable because of the proposed α1 positioning and the fewer types of interactions required for the rosette assembly in the plasma membrane.

Indeed, the protein−protein interaction mechanism of rosette assembly is not yet understood. The *N*-terminal zinc finger domain of CesA protein under oxidized conditions has been proposed to be responsible for formation of CesA homodimers or heterodimers (*42*). For precise assembly, a more specific interaction mechanism might be expected! There is no direct biochemical evidence yet to confirm how the rosettes are assembled; probably the zinc finger domains of CesA proteins, the plasma membrane, and microtubules are all involved.

We propose that, during the spontaneous assembly of the rosettes, the α1 molecule from each asymmetric subunit is always indexed to the center of the rosettes to ensure the correct positioning of each of the three types of CesA proteins. On the basis of our modified rosettes model, the rosette assembly probably starts with the dimerization (β−β) of the *N*-terminal zinc finger domain of CesAs. The next step is an α−β interaction, with each α isoform interacting with two β isoforms. Here as well, there is no direct evidence yet to prove how cells control these interactions among the catalytic units. One possibility is that different protein−protein interactions (i.e. β−β and α−β) occur under different physiological conditions or in different locations in the cell. Experiments of *in vitro* assembly or *in vivo* labeling of coexpressed CesA proteins might confirm this hypothesis.

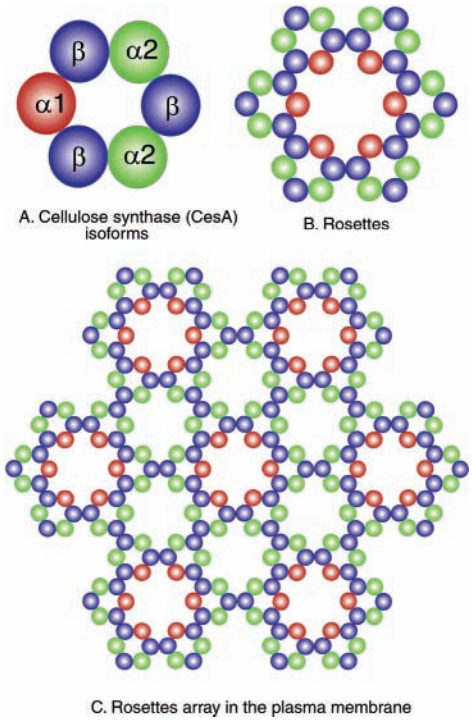

Figure 3. Schematic model structure of the cellulose synthases complex (rosettes) in higher plants. 36 CesA proteins assemble into rosettes containing six identical subunits; each subunit (**A**) is composed of six CesA proteins (one α1, two α2, and three β isoforms); a number of rosettes (**B**) form a honeycomb array (**C**) in the plasma membrane. Three types of protein–protein interaction may be involved in the spontaneous assembly: α1–β, α2–β, and β–β. Each CesA protein catalyzes one β-glucan chain, the rosettes synthesize 36 chains of one elementary fibril, and the locus of honeycomb arrayed rosettes synthesizes a number of elementary fibrils to form a macrofibril.

There is little progress in measuring the cellulose synthase activity *in vitro* (*43*, *44*). It is commonly assumed that the 36-chain elementary fibril is synthesized by hexagonal rosettes containing 36 CesA proteins, where each CesA enzyme produces one β-D-glucan chain (*7*). The diversity of rosettes may imply two aspects of the synthesis process: first, to produce variants of elementary fibril structure in different cell wall types and their developmental stages (i.e. primary and secondary wall biosynthesis), and second, to perform at different catalytic rates.

Cellulose Crystallite Structure—Biophysical Clues. Various approaches have been used to measure the chemical and physical properties of plant cell wall crystalline cellulose. In brief, the cellulose from higher plants contains Iα- and Iβ-like crystalline allomorphs with disordered surface chains (*11*, *16*). Because of the small size (only 2−3 nm) of the cellulose crystallite and the tendency to form a complex interaction network (associated with other noncrystalline polysaccharides) among cell wall matrixes, there is little known about the molecular structure of the native cell wall cellulose fiber. The challenges not only come from the limited resolution of available measurement techniques, but also come from cellulose sample preparation processes. To isolate microfibrils from the plant cell wall, sequential extraction processes using acid and alkaline incubations are usually involved, sometimes at high temperature. We suspect that, because of the extensive sample preparation, most if not all of

the microfibrils described in the previous literature were in fact modified fiber aggregates (*45*). Measurements of single treated "microfibrils" using TEM have revealed cross-sectional dimensions of about 2−3 nm. This "microfibril" is actually the cellulose crystallite plus a small amount of damaged (altered) noncrystalline polysaccharides associated with its surface. This conclusion is also supported by studies of higher-plant cellulose crystallites using ^{13}C solid-state NMR (*11*) and FTIR (*46*). These data furthermore suggested a Iβ-like crystal structure with Iα-like chains (*16*). Vietor and co-workers (*47*) found that the C-6 position of surface chains differs from that of internal chains, altering the H-bond from O2 to O6 for surface chains, thereby changing the conformation of surface glucose residues (*16*, *47*, *48*). The question remains, how does this extensively treated "microfibril" relate to its native form in the plant cell wall?

Elementary Fibril, Macrofibril, and Microfibril—New Findings from AFM. To characterize the native cell wall structure, traditional extraction processes must be eliminated to minimize possible cell wall modification during sample preparation. In our AFM study of the maize parenchyma cell wall, we were able to image the native structure of different faces of a given cell, as well as different cells. The minimum size of the microfibril from the AFM *z*-axis (height image) is about 5×10 nm^2, which is similar to those measured from the primary cell walls of onion (*Allium cepa*) and *Arabidopsis thaliana* (*29*). Because the primary cell wall is a dynamic system and the microfibril lamellae are always undergoing modification during cell growth, accurate measurements of the dimensions of the microfibril may not be obtainable. The most interesting discovery from our high-resolution AFM study is the diversity of fibillar structures imaged on the native primary cell walls.

The direct imaging of macrofibrils and microfibrils leads us to a new hypothesis of how microfibrils are synthesized during cell growth. We observed that the macrofibril exists only on the uppermost surface layer of the cell wall, the layer adjacent to the plasma membrane. We feel it is unlikely that the "macrofibril" feature is caused by the cell wall drying process. Macrofibrils seem to initiate from one locus and appear to split or fray at the opposite (distal) end, which implies that the macrofibril is a bundle of newly synthesized elementary fibrils. We therefore speculate that the cell walls with macrofibrils are from growing cells. If that is true, a sequential fiber synthesis process could be proposed, which consists of the following: elementary fibril → macrofibril → microfibril. Because of the sticky (high-energy) surfaces of the elementary fibrils, when a number of elementary fibrils are synthesized simultaneously, they immediately coalesce to form the macrofibril. The macrofibril disperses at the distal end to form parallel-arranged microfibrils. During later cell maturation, more polymers (hemicelluloses/pectin) and other wall components are deposited on the microfibril surface. The microfibrils become almost undetectable on the mature cell wall, as shown in **Figure 1I**.

New 36-Chain Model of the Elementary Fibril. Several microfibril structure models have been proposed over a 30-year span (*19*, *49*). In most of these models, cellulose was assumed to form a crystalline core structure and hemicelluloses were assumed to interact with the cellulose surfaces to form the noncrystalline sheath. This cellulose/hemicellulose network determines the stiffness of the plant cell wall. Earlier, Preston and Cronshaw (*50*) suggested a core/sheath chain arrangement model. In their model, the microfibril had a rectangular shape of 5×10 nm^2 in cross section and was composed of an ordered central core and a paracrystalline sheath.

From the above discussion, we have proposed a new molecular model based on a 36-chain elementary fibril. **Figure 4** shows the schematic molecular structure of the proposed 36-chain elementary fibril model (**Figure 4A and B**), the macrofibril (**Figure 4C**), and the microfibril (**Figure 4D and E**). In this model, the elementary fibril refers to the original structure synthesized by the rosettes containing 36-glucan chains. The macrofibril refers to the bundle structure formed by a number of elementary fibrils synthesized from one locus. The microfibril refers to the structure containing one elementary fibril and various amounts of hemicelluloses coated on its surface. There is no biochemical evidence yet to support the concept that non-cellulose polysaccharide synthase is involved in the assembly of rosettes. Thus, we assume that all 36 glucan chains of the elementary fibril are cellulose. The experimental measurements have suggested that the cellulose crystallite in higher plants is only 2−3 nm, which is less than 36 chains (the elementary fibril) based on the available model cellulose I crystal structures. Šturcová and co-workers (*16*) have suggested that higher plants synthesize cellulose Iβ; however, the chain conformation is similar to that of Iα, based on the NMR data. We therefore propose that the elementary fibril is a heterogeneous structure containing a crystalline core and layers of subcrystalline/paracrystalline sheaths. The conformational differences of the glucose residues in each glucan are probably the primary factors responsible for those structural disorders. The crystalline core displays a Iβ structure. Theoretically, the cellulose crystallite cross section could be as small as 1.5×2 nm^2 (six group-C chains) to a maximum of 3×5 nm^2 (all 36 chains), calculated on the basis of the model cellulose Iβ crystal structure. In most cases, the crystallite size would be between $1.5-3 \times 3-5$ nm^2 in cross section. Our speculation about cellulose crystallite size is consistent with data measured by TEM or other experimental approaches (*11*). Although it is difficult to investigate experimentally, the best local structures for these cellulose chains may have come from solid-state ^{13}C NMR, which suggested that structural disorders (i.e., the different C6 position alters the intramolecular hydrogen bond at O6−O2) exist in surface chains (*47*). Recently, we conducted computer simulations using an integrated quantum mechanical approach that suggests that the cellulose crystal has high energy at the surfaces of both the Iα and Iβ allomorphic domains. Cellulose may tend to reform into larger structures unless structural disorders are introduced into the crystal surface (*51*).

In this model, the 36 glucan chains are categorized into three groups according to their position (**Figure 4B**): (1) a center true-crystal core (group-C1, Ch1−6), (2) chains immediately associated with the crystal core (group-C2, Ch7−18), and (3) surface chains (group-C3, Ch19−36). The groups-C2 and −C3 form protection and transition phases between the crystalline core and later-deposited noncrystalline polymers during microfibril biosynthesis. The group-C1 chains (Ch1−6) are considered truly crystalline in this model. We postulate that it is structurally similar to the model cellulose Iβ, with Ch1 and Ch4 being the two surface chains and Ch2/Ch6 and Ch3/Ch5 forming two alternative sheets. The planar faces (1,0,0) and (−1,0,0) contain only one chain each, Ch1 and Ch4, respectively. In the traditional cellulose Iβ crystal structure model, two types of chain conformation are recognized, the "origin" and the "center" chains. Corresponding to our model, the origin conformation includes chains Ch1, -3, and -5, and the center conformation includes chains Ch2, -4, and -6. This conformational difference may generate a potentially polarized structure, which may in turn direct the lateral orientation of the cellulose

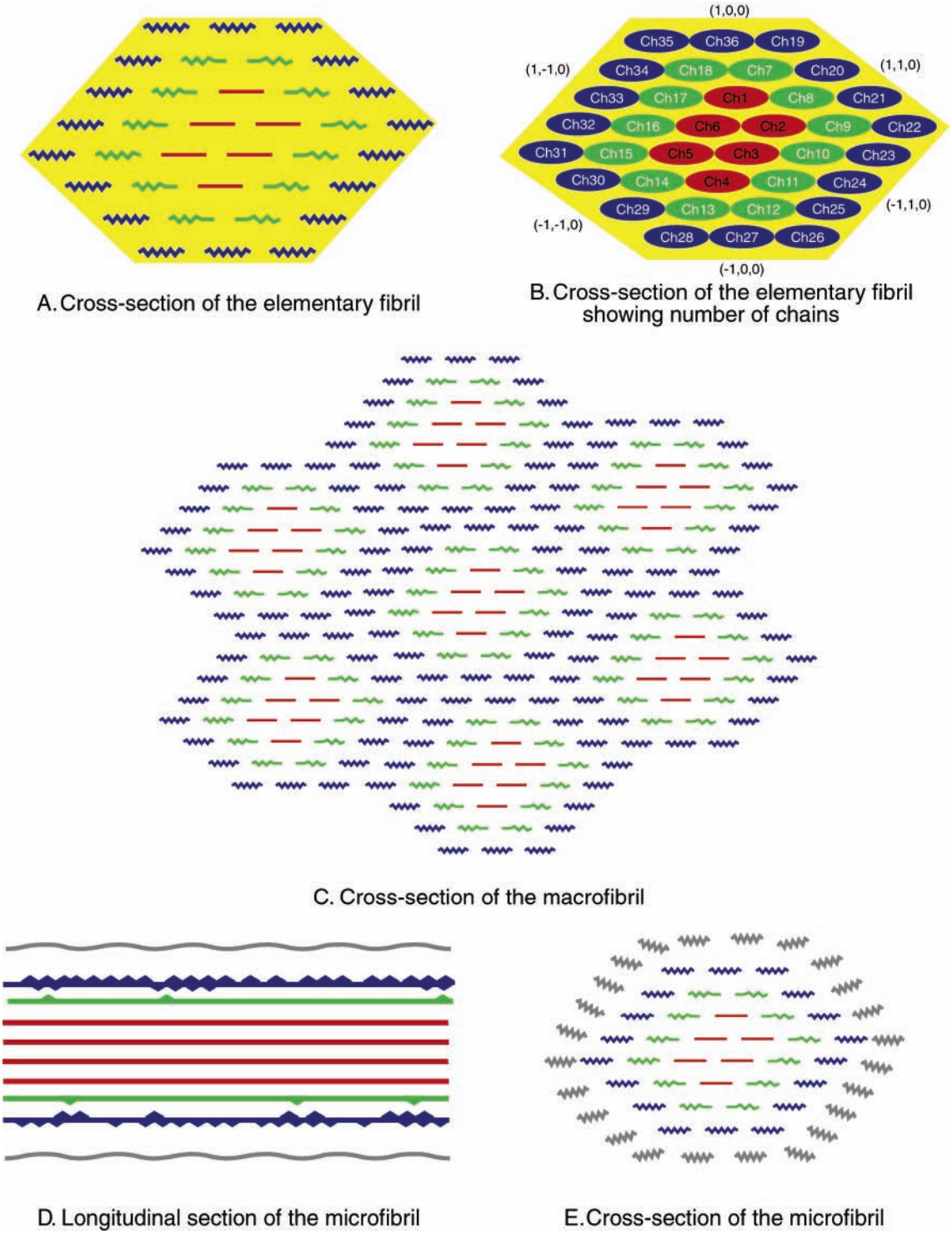

Figure 4. Molecular structural models of the 36-chain elementary fibril, the macrofibril, and the microfibril. **(A)** Cross section of the elementary fibril containing 36 glucan chains. Crystalline chains are indicated as a straight line; noncrystalline and subcrystalline chains are indicated as wavy lines. We propose that the 36 glucan chains are packed similarly to the cellulose Iβ model. **(B)** Chains are numbered from Ch1 to Ch36 and categorized into three groups: group-C1 (red) contains six true crystalline chains, group-C2 (green) contains twelve subcrystalline chains, and group-C3 (blue) contains 18 subcrystalline or noncrystalline chains. **(C)** The macrofibril is formed by elementary fibrils synthesized from one locus of a number of honeycomb-arrayed rosettes. During cell growth, the macrofibril eventually splits into single microfibrils coated with hemicelluloses (**D** and **E**). **(D)** Longitudinal section of the microfibril. Hemicelluloses (gray wavy lines) are coated on the surface of the elementary fibril to form a stiffness microfibril network in higher plant cell walls. **(E)** Cross section of the microfibril. The chain conformation of the elementary fibril could also be altered during this process (see detailed discussion in the text).

crystallite in the elementary fibril, which could then be continued on to the structures of the macrofibrils and microfibrils in the plant cell wall matrixes. Note that the six crystalline core chains shown in **Figure 4** form a hexagonal cross section. Importantly, we detected no periodic disruption along the length of the microfibrils by AFM. This may indicate that the crystalline core is longitudinally continuous without the amorphous interruption (paracrystalline regions) proposed by some early studies.

The twelve group-C2 chains (Ch7−18) are immediately associated with the surface of the crystal core, forming a sheath around it. Since the group-C2 chains form the transitional phase between the crystalline group-C1 and subcrystalline group-C3, the chain conformation of group-C2 largely relies on group-C2 chains. The group-C2 chains could be nearly full crystalline or subcrystalline depending on the crystallinity of group-C3 chains. The chain edge close to the group-C1 chains may be fixed by intermolecular H-bonds (O3′−O5 and O2−O6′), whereas the other edge may have more structural disorders due to interaction with the group-C3 chains. The eighteen group-C3 (Ch19−Ch36) chains are all surface chains forming the second layer of the sheath around the crystal cellulose core. This layer may keep some level of crystalline structure in high-cellulose-content tissue. In most other cases, we propose that they are all noncrystalline. It is also important to note that the elementary fibril does not exist independently in nature. The group-C3 chains interact either with the other group-C3 chains of the neighboring elementary fibril (as in the macrofibril) or with hemicelluloses in the microfibril. In the latter case, the chain conformation could be altered dramatically by surface interactions with hemicelluloses during biosynthesis (i.e., from the elementary fibril to a microfibril). Regardless of which polymers are coated on the elementary fibril surface, eventually the overall crystallinity decreases from the center to group-C2 and -C3 layers. Elementary fibrils joined in macrofibrils would therefore have the maximum size of the crystallite; indeed, the faceting morphology we observed for the macrofibril may support that it is a highly crystalline bundle of uncoated elementary fibrils.

We do not know how plants control molecular structural variation of elementary fibrils during their biosynthesis. In our new 36-chain cellulose model, we make the following speculations: (1) the 36 cellulose chains are not polymerized simultaneously (timing); (2) the 36 chains are synthesized by different CesA proteins assembled in certain positions (spacing) in the rosettes; and (3) the three groups of chains (C1, C2, and C3) may be synthesized by three types of CesA proteins (rosette assembly). One type of CesA protein (probably α1) is responsible for the synthesis of the cellulose crystalline core that has to be positioned in the center area during rosette assembly. The twelve α2-type CesA proteins polymerize the twelve group-C2 chains. The eighteen β-type CesA proteins catalyze the eighteen group-C3 chains. The elementary fibril could also be modified prior to macrofibril assembly and later by hemicellulose deposition during microfibril formation. Enzymes other than CesAs may also be involved in the elementary fibril biosynthesis process; for example, an endoglucanase (Korrigan) has been definitely linked to cellulose synthesis (*8*).

Cell elongation and cell wall loosening are probably much more dynamic, the cell turgor pressure is thought to generate the primary expansive forces, and a cascade of enzymes are involved in these processes (*2*). In general, during cell growth the cellulose synthesis occurs in the plasma membrane, while non-cellulosic wall components (hemicellulose/pectin) secrete from the Golgi vesicles. The macrofibril contains a number of elementary fibrils synthesized simultaneously from one locus. During cell growth, the macrofibril starts loosening at its end, the single elementary fibrils split, and the hemicellulose coating begins to form, all simultaneously to form the parallel arrays of microfibrils we observe by AFM. During the cell wall elongation process, more elementary fibrils tear off or unwrap from their source macrofibril (see **Figure 1F**). Microfibrils are then cross-linked by hemicelluloses/pectin to form a new cell wall lamella. In our elementary fibril model, the structurally disordered group-C3 chains may be the loosening point for the macrofibril.

More than a dozen glycosyl residues and various glycosidic-bond linkages have been reported in the polysaccharides found in the primary cell walls of higher plants. By introducing these variations into the polysaccharides directly associated with cellulose during microfibril biosynthesis, the molecular structure of the microfibril, although cellulose Iα and Iβ terms are still used here, is probably dynamic, especially the transition phases (group-C2 and -C3 chains in the elementary fibril). The crystallinity of the elementary fibril might be altered when the microfibril is forming, depending on which hemicelluloses are deposited on its surface.

Conclusion. We have proposed a new model of a 36-chain elementary fibril and its biosynthesis based on our direct AFM imaging of the maize parenchyma cell wall surface and a detailed review of reported experimental evidence. We now assume that the elementary fibril is synthesized from rosettes containing 36 CesA proteins that produce 36 β-D-glucans in higher plants. These 36 glucan chains then assemble through hydrogen bonding and van der Waals forces to form a crystalline core and the subcrystalline shell structure of the elementary fibril. Although we postulate only cellulose in our 36-chain elementary fibril model, one question still remains: does the composition of the elementary fibril change during cell wall growth? Recall that TEM and NMR have estimated the cellulose crystallite in higher plants as only 2−3 nm in diameter with disordered surface chains. Note that TEM requires solvent extractions that can remove noncrystalline layers (i.e., hemicelluloses, noncrystalline cellulose, and other polymers) and NMR provides quantitative measurements of crystalline cellulose content. It is not yet confirmed that these structural disorders indeed exist in the native plant cell wall microfibril or are caused by the extraction process during sample preparation. It is unlikely, but not impossible, that non-cellulosic polysaccharides (i.e. with different glycosyl bonds and residues) could be involved in group-C3 chains of the elementary fibril. Several research groups have reported that the mixed β-(1,3)-(1,4)-D-glucan (*52*−*54*) mannan synthases (*55*) are phylogenetically grouped in the same superfamily as cellulose synthases.

Although still speculative in detailed concepts, we believe the new model provides the first molecular level vision of the elementary fibril that can be extended to the formation of microfibrils and macrofibrils in the primary cell walls of higher plants. Future evidence for this model will come from direct characterization of the plant cell wall surface structure using specific molecular probes. For example, functionalized AFM tips can be used to probe the molecular structure of cell wall polysaccharides, detailed biochemistry studies of CesA protein regulation will tell more about cellulose synthesis, and studying the energetics of cellulose association processes using molecular dynamics computer simulations will help us understand more about the assembly and structure of the elementary fibril.

ACKNOWLEDGMENT

The authors wish to thank Dr. Xianghong Qian for valuable discussions concerning computer simulations of polysaccharides.

LITERATURE CITED

(1) Nelson, R. G.; Walsh, M.; Sheehan, J. J.; Graham, R. Methodology for estimating removable quantities of agricultural residues for bioenergy and bioproduct use. *Appl. Biochem. Biotechnol.* **2004**, *113*−*16*, 13−26.

(2) Cosgrove, D. J. Wall structure and wall loosening. A look backwards and forwards. *Plant Physiol.* **2001**, *125* (1), 131−134.
(3) Carpita, N. C.; Defernez, M.; Findlay, K.; Wells, B.; Shoue, D. A.; Catchpole, G.; Wilson, R. H.; McCann, M. C. Cell wall architecture of the elongating maize coleoptile. *Plant Physiol.* **2001**, *127* (2), 551−565.
(4) Somerville, C.; Bauer, S.; Brininstool, G.; Facette, M.; Hamann, T.; Milne, J.; Osborne, E.; Paredez, A.; Persson, S.; Raab, T.; Vorwerk, S.; Youngs, H. Toward a systems approach to understanding plant-cell walls. *Science* **2004**, *306* (5705), 2206−2211.
(5) Vincent, J. F. V. From cellulose to cell. *J. Exp. Biol.* **1999**, *202* (23), 3263−3268.
(6) Rose, J. K. C. *The Plant Cell Wall: Annual Plant Reviews*; Blackwell Publishing: Garsington, 2003; Vol. 8.
(7) Brown, R. M.; Saxena, I. M. Cellulose biosynthesis: A model for understanding the assembly of biopolymers. *Plant Physiol. Biochem.* **2000**, *38* (1−2), 57−67.
(8) Doblin, M. S.; Kurek, I.; Jacob-Wilk, D.; Delmer, D. P. Cellulose biosynthesis in plants: from genes to rosettes. *Plant Cell Physiol.* **2002**, *43* (12), 1407−1420.
(9) Ohad, I.; Danon, D.; Hestrin, S. Synthesis of cellulose by *Acetobacter xylium*: V. Ultrastructure of polymer. *J. Cell Biol.* **1962**, *12*, 31−46.
(10) Ohad, I.; Danon, D. On the dimensions of cellulose microfibrils. *J. Cell Biol.* **1964**, *22*, 302−305.
(11) Ha, M. A.; Apperley, D. C.; Evans, B. W.; Huxham, M.; Jardine, W. G.; Vietor, R. J.; Reis, D.; Vian, B.; Jarvis, M. C. Fine structure in cellulose microfibrils: NMR evidence from onion and quince. *Plant J.* **1998**, *16* (2), 183−190.
(12) Emons, A. M. C. Methods for visualizing cell-wall texture. *Acta Bot. Neerl.* **1988**, *37* (1), 31−38.
(13) Mccann, M. C.; Wells, B.; Roberts, K. Direct visualization of cross-links in the primary plant-cell wall. *J. Cell Sci.* **1990**, *96*, 323−334.
(14) Jarvis, M. C. Solid-state ^{13}C-n.m.r. spectra of vigna primary cell walls and their polysaccharide components. *Carbohydr. Res.* **1990**, *201* (2), 327−333.
(15) Lehtio, J.; Sugiyama, J.; Gustavsson, M.; Fransson, L.; Linder, M.; Teeri, T. T. The binding specificity and affinity determinants of family 1 and family 3 cellulose binding modules. *Proc. Natl. Acad. Sci. USA* **2003**, *100* (2), 484−489.
(16) Šturcová, A.; His, I.; Apperley, D. C.; Sugiyama, J.; Jarvis, M. C. Structural details of crystalline cellulose from higher plants. *Biomacromolecules* **2004**, *5* (4), 1333−1339.
(17) Sugiyama, M.; Hara, K.; Hiramatsu, N.; Iijima, H. Small-angle neutron scattering observation of aqueous suspension of microcrystalline cellulose. *Jpn. J. Appl. Phys., Part 2* **1998**, *37* (4A), L404−L405.
(18) Sene, C. F. B.; Mccann, M. C.; Wilson, R. H.; Grinter, R. Fourier transform Raman and Fourier transform infrared-spectroscopy—an investigation of 5 higher-plant cell-walls and their components. *Plant Physiol.* **1994**, *106* (4), 1623−1631.
(19) Mühlethaler, K. Ultrastructure and formation of plant cell walls. *Annu. Rev. Plant Physiol.* **1967**, *18*, 1−24.
(20) Nishiyama, Y.; Sugiyama, J.; Chanzy, H.; Langan, P. Crystal structure and hydrogen bonding system in cellulose Iα, from synchrotron X-ray and neutron fiber diffraction. *J. Am. Chem. Soc.* **2003**, *125* (47), 14300−14306.
(21) Nishiyama, Y.; Langan, P.; Chanzy, H. Crystal structure and hydrogen-bonding system in cellulose Iβ from synchrotron X-ray and neutron fiber diffraction. *J. Am. Chem. Soc.* **2002**, *124* (31), 9074−9082.
(22) Atalla, R. H.; VanderHart, D. L. Native cellulose—a composite of 2 distinct crystalline forms. *Science* **1984**, *223*, 283−285.
(23) Sugiyama, J.; Persson, J.; Chanzy, H. Combined IR and electron diffraction study of the polymorphism of native cellulose. *Macromolecules* **1991**, *24*, 2461−2466.
(24) Atalla, R. H.; VanderHart, D. L. The role of solid-state ^{13}C NMR spectroscopy in studies of the nature of native celluloses. *Solid State Nucl. Magn. Reson.* **1999**, *15*, 1−19.
(25) Baker, A. A.; Helbert, W.; Sugiyama, J.; Miles, M. J. High-resolution atomic force microscopy of native *Valonia* cellulose I microcrystals. *J. Struct. Biol.* **1997**, *119* (2), 129−138.
(26) Baker, A. A.; Helbert, W.; Sugiyama, J.; Miles, M. J. New insight into the structure of the cellulose surface by AFM reveals the I-α phase and suggests a modified hydroxymethyl conformation. *Abstr. Pap. Am. Chem. Soc.* **2000**, *219*, U260−U260.
(27) Kirby, A. R.; Gunning, A. P.; Waldron, K. W.; Morris, V. J.; Ng, A. Visualization of plant cell walls by atomic force microscopy. *Biophys. J.* **1996**, *70* (3), 1138−1143.
(28) Morris, V. J.; Gunning, A. P.; Kirby, A. R.; Round, A.; Waldron, K.; Ng, A. Atomic force microscopy of plant cell walls, plant cell wall polysaccharides and gels. *Int. J. Biol. Macromol.* **1997**, *21* (1−2), 61−66.
(29) Davies, L. M.; Harris, P. J. Atomic force microscopy of microfibrils in primary cell walls. *Planta* **2003**, *217* (2), 283−289.
(30) Urbanowicz, B. R.; Rayon, C.; Carpita, N. C. Topology of the maize mixed linkage (1 → 3),(1 → 4)-beta-D-glucan synthase at the Golgi membrane. *Plant Physiol.* **2004**, *134* (2), 758−768.
(31) Burton, R. A.; Shirley, N. J.; King, B. J.; Harvey, A. J.; Fincher, G. B. The CesA gene family of barley. Quantitative analysis of transcripts reveals two groups of coexpressed genes. *Plant Physiol.* **2004**, *134* (1), 224−236.
(32) Holland, N.; Holland, D.; Helentjaris, T.; Dhugga, K. S.; Xoconostle-Cazares, B.; Delmer, D. P. A comparative analysis of the plant cellulose synthase (CesA) gene family. *Plant Physiol.* **2000**, *123* (4), 1313−1323.
(33) Tanaka, K.; Murata, K.; Yamazaki, M.; Onosato, K.; Miyao, A.; Hirochika, H. Three distinct rice cellulose synthase catalytic subunit genes required for cellulose synthesis in the secondary wall. *Plant Physiol.* **2003**, *133* (1), 73−83.
(34) Richmond, T. A.; Somerville, C. R., Integrative approaches to determining Csl function. *Plant Mol. Biol.* **2001**, *47* (1−2), 131−143.
(35) Arioli, T.; Peng, L. C.; Betzner, A. S.; Burn, J.; Wittke, W.; Herth, W.; Camilleri, C.; Hofte, H.; Plazinski, J.; Birch, R.; Cork, A.; Glover, J.; Redmond, J.; Williamson, R. E. Molecular analysis of cellulose biosynthesis in *Arabidopsis*. *Science* **1998**, *279* (5351), 717−720.
(36) Mueller, S. C.; Brown, R. M.; Scott, T. K. Cellulosic microfibrils − Nascent stages of synthesis in a higher plant-cell. *Science* **1976**, *194*, 949−951.
(37) Emons, A. M. C. Role of particle rosettes and terminal globules in cellulose synthesis. In *Biosynthesis and Biodegradation of Cellulose*; Haigler, C. H., Weimer, P. J., Eds.; Marcel Dekker: New York, 1991; p 71−98.
(38) Kimura, S.; Laosinchai, W.; Itoh, T.; Cui, X. J.; Linder, C. R.; Brown, R. M. Immunogold labeling of rosette terminal cellulose-synthesizing complexes in the vascular plant *Vigna angularis*. *Plant Cell* **1999**, *11* (11), 2075−2085.
(39) Taylor, N. G.; Howells, R. M.; Huttly, A. K.; Vickers, K.; Turner, S. R. Interactions among three distinct CesA proteins essential for cellulose synthesis. *Proc. Natl. Acad. Sci. USA* **2003**, *100* (3), 1450−1455.
(40) Perrin, R. M. Cellulose: How many cellulose synthases to make a plant? *Curr. Biol.* **2001**, *11* (6), R213−R216.
(41) Scheible, W. R.; Eshed, R.; Richmond, T.; Delmer, D.; Somerville, C. Modifications of cellulose synthase confer resistance to isoxaben and thiazolidinone herbicides in *Arabidopsis Ixr1* mutants. *Proc. Natl. Acad. Sci. USA* **2001**, *98* (18), 10079−10084.
(42) Kurek, I.; Kawagoe, Y.; Jacob-Wilk, D.; Doblin, M.; Delmer, D. Dimerization of cotton fiber cellulose synthase catalytic subunits occurs via oxidation of the zinc-binding domains. *Proc. Natl. Acad. Sci. USA* **2002**, *99* (17), 11109−11114.

(43) Lai-Kee-Him, J.; Chanzy, H.; Muller, M.; Putaux, J. L.; Imai, T.; Bulone, V. *In vitro versus in vivo* cellulose microfibrils from plant primary wall synthases: Structural differences. *J. Biol. Chem.* **2002**, *277* (40), 36931−36939.

(44) Okuda, K.; Li, L. K.; Kudlicka, K.; Kuga, S.; Brown, R. M. β-Glucan synthesis in the cotton fiber. 1. Identification of β-1,4-glucan and β-1,3-glucan synthesized *in vitro*. *Plant Physiol.* **1993**, *101* (4), 1131−1142.

(45) Ranby, B. G. The colloidal properties of cellulose micelles. *Discuss. Faraday Soc.* **1951**, *11*, 158−164.

(46) Åkerholm, M.; Hinterstoisser, B.; Salména, L. Characterization of the crystalline structure of cellulose using static and dynamic FT-IR spectroscopy. *Carbohydr. Res.* **2004**, *339* (3), 569−578.

(47) Vietor, R. J.; Newman, R. H.; Ha, M. A.; Apperley, D. C.; Jarvis, M. C. Conformational features of crystal-surface cellulose from higher plants. *Plant J.* **2002**, *30* (6), 721−731.

(48) Bootten, T. J.; Harris, P. J.; Melton, L. D.; Newman, R. H. Solid-state ^{13}C-NMR spectroscopy shows that the xyloglucans in the primary cell walls of mung bean (*Vigna radiata L.*) occur in different domains: a new model for xyloglucan-cellulose interactions in the cell wall. *J. Exp. Bot.* **2004**, *55* (397), 571−583.

(49) Brown, R. M. Cellulose structure and biosynthesis: What is in store for the 21st century? *J. Polym. Sci., Polym. Chem.* **2004**, *42* (3), 487−495.

(50) Preston, R. D.; Cronshaw, J. Constitution of the fibrilar and nonfibrillar Components of the Walls of *Valonia* ventricosa. *Nature* **1958**, *181*, 248−250.

(51) Qian, X.; Ding, S.-Y.; Nimlos, M. R.; Johnson, D. K.; Himmel, M. E. The atomic and electronic structures of molecular crystalline cellulose Iβ − a first-principles investigation. *Macromolecules* **2005**, *38* (25), 10580−10589.

(52) Dhugga, K. S. Building the wall: genes and enzyme complexes for polysaccharide synthases. *Curr. Opin. Plant Biol.* **2001**, *4* (6), 488−493.

(53) Dhugga, K. S. Plant Golgi cell wall synthesis: From genes to enzyme activities. *Proc. Natl. Acad. Sci. USA* **2005**, *102* (6), 1815−1816.

(54) Vergara, C. E.; Carpita, N. C. beta-D-Glycan synthases and the CesA gene family: lessons to be learned from the mixed-linkage (1 → 3),(1 → 4)beta-D-glucan synthase. *Plant Mol. Biol.* **2001**, *47* (1−2), 145−160.

(55) Dhugga, K. S.; Barreiro, R.; Whitten, B.; Stecca, K.; Hazebroek, J.; Randhawa, G. S.; Dolan, M.; Kinney, A. J.; Tomes, D.; Nichols, S.; Anderson, P. Guar seed beta-mannan synthase is a member of the cellulose synthase super gene family. *Science* **2004**, *303* (5656), 363−366.

Received for review July 28, 2005. Revised manuscript received November 29, 2005. Accepted December 8, 2005. This work was funded by the U.S. DOE Office of the Biomass Program.

JF051851Z